Hindawi
Journal of Nanomaterials
Volume 2017, Article ID 5385908, 8 pages
https://doi.org/10.1155/2017/5385908

Research Article

Synthesis, Characterization, and Catalytic Performance of Sb_2Se_3 Nanorods

Ning Hu,[1] Marcos A. Cheney,[2] Younes Hanifehpour,[3] Sang Woo Joo,[3] and Bong-Ki Min[4]

[1]*Key Laboratory of Biorheological Science and Technology, Ministry of Education and Key Lab of Visual Damage and Regeneration and Restoration of Chongqing, Bioengineering College, Chongqing University, Chongqing 400030, China*
[2]*University of Maryland Eastern Shore, Princess Anne, MD 21853, USA*
[3]*School of Mechanical Engineering, WCU Nano Research Center, Yeungnam University, Gyeongsan 712-749, Republic of Korea*
[4]*Center for Research Facilities, Yeungnam University, Gyeongsan 712-749, Republic of Korea*

Correspondence should be addressed to Ning Hu; huning@cqu.edu.cn, Marcos A. Cheney; macheney@umes.edu, and Sang Woo Joo; swjoo1@gmail.com

Received 19 January 2017; Revised 22 March 2017; Accepted 2 April 2017; Published 4 July 2017

Academic Editor: Yasuhiko Hayashi

Antimony selenide has many potential applications in thermoelectric, photovoltaic, and phase-change memory devices. A novel method is described for the rapid and scalable preparation of antimony selenide (Sb_2Se_3) nanorods in the presence of hydrazine hydrate and/or permanganate at 40°C. Crystalline nanorods are obtained by the addition of hydrazine hydrate in a reaction mixture of antimony acetate and/or chloride and sodium selenite in neutral and basic media, while amorphous nanoparticles are formed by the addition of $KMnO_4$ in a reaction mixture of antimony acetate/chloride and sodium selenite. The powder X-ray diffraction pattern confirms orthorhombic phase crystalline Sb_2Se_3 for the first and second reactions with lattice parameters $a = 1.120$ nm, $b = 1.128$ nm, and $c = 0.383$ nm and amorphous Sb_2Se_3 for the third reaction. Scanning electron microscopy (SEM), transmission electron microscopy (TEM), and high-resolution TEM (HRTEM) images show the diameter of nanorods for the first and second reactions to be in the order of 100 nm to 150 nm and about 20 nm particles for the third reaction. EDX and XPS suggest that the nanorods are pure Sb_2Se_3. The UV-vis analysis indicates a band gap of 4.14 and 4.97 eV for the crystalline and amorphous Sb_2Se_3, respectively, corresponding to a blue shift. The photocatalytic study shows that the decolorization of Rhodamine in solution by nanoparticles is slightly greater than nanorods.

1. Introduction

Structure, morphology, and composition of nanorods and nanoparticles are important parameters that give rise to their properties and thus applications. Morphological and structural changes associated with semiconducting V2VI3 compounds such as Sb_2Se_3 are not well understood.

The semiconducting V_2VI_3 compounds (Sb_2S_3 and Sb_2Se_3) are highly anisotropic semiconductors with a layered structure parallel to the growth direction with orthorhombic phase crystal structure, which is known to adopt a number of packing structures resulting in either trigonal prismatic or octahedral coordination of the metals within a layered matrix of chalcogens [1]. Semiconductor selenides find applications as laser materials, optical filters, sensors, and solar cells. Antimony selenide, an important member of these V_2VI_3 compounds, is a layer-structured semiconductor of orthorhombic crystal structure and exhibits good photovoltaic properties and high thermoelectric power (TEP) which allows possible applications for optical and thermoelectronic cooling devices [2–7]. Over the past two decades, many methods have been employed to prepare Sb_2Se_3 nanotubes, nanoribbons, nanowires, nanosheets, nanorods, nanobelts, nanospheres, and nanoflakes, including thermal decomposition [8, 9], complex decomposition approach [10], solvothermal reaction [11, 12], microwave irradiation [13], vacuum evaporation [14], and other chemical reaction approaches [15, 16]. However, most of the reports were focused on the preparation of Sb_2Se_3

with reaction times much more than 10 h [17–22]. Hence, the synthesis of 1D nanomaterials in high yield via a quick process is still a challenge. In this study, antimony selenide (Sb_2Se_3) nanomaterials with uniform size and morphology are prepared by a soft hydrothermal process using hydrazine hydrate and permanganate in just 30 min. The surprising morphological and structural changes occurring in the presence of permanganate are also presented. The present route is simple, cost-effective, and reproducible.

2. Experimental Section

2.1. Synthesis. All chemicals were of analytical grade and were used as received. All glassware were acid-cleaned, and the ultrapure water was devoid of any trace of organics. The synthesis of Sb_2Se_3 is performed by a new redox method using antimony acetate and/or chloride salts, sodium selenite, hydrazine hydrate ($N_2H_4{\cdot}H_2O$), and/or permanganate in neutral and basic aqueous solution, respectively. For the first reaction, $Sb(CH_3COO)_3$ (0.227 g, 0.750 mmol) and Na_2SeO_3 (0.259 g, 1.49 mmol) were weighted independently and then placed together into a 50 mL volumetric flask followed by the addition of 25 mL of pure water at room temperature. It is important to dissolve all the salts simultaneously via sonication to obtain the results desired. After the salts were completely dissolved, 3 mL of 80% hydrazine hydrate and NaOH (0.01 mol, pH = 10) is added dropwise to the solution followed by dilution to the 50 mL mark with pure water and then placed in a sonicator bath at 40°C for 40 min. After the addition of hydrazine, the solution turned turbid, and a white/beige precipitate appeared, which rapidly settled down, leaving a colorless solution. The solids are separated by filtration (Whatman filter paper) and washed with ethanol and pure water, followed by air drying at room temperature for characterization. The first reaction is summarized as

$$\begin{aligned} &2Sb\left(CH_3COO\right)_3\left(aq\right) + 3Na_2SeO_3\left(aq\right) \\ &\xrightarrow{N_2H_4+NaOH} Sb_2Se_3\left(s\right) + N_2 + H_2O + 6Na^+ \\ &\qquad + 6CH_3COO^- + NH_3 \end{aligned} \tag{1}$$

Note that we run the above reaction in the absence of NaOH as well. Since there were no noticeable differences in the color of the product with and without NaOH, we proceeded to change the salt type of the reaction. The only difference observed was in the amount of solids produced which were more in the presence of NaOH.

For the second reaction, the above process was repeated, except that $SbCl_3$ was used in place of $Sb(CH_3COO)_3$ with no NaOH, to study the effect of salt type and pH on the reaction. In this case, the solids produced are black:

$$\begin{aligned} &2SbCl_3\left(aq\right) + 3Na_2SeO_3\left(aq\right) \\ &\xrightarrow{N_2H_4} Sb_2Se_3\left(s\right) + N_2 + H_2O + 6Cl^- + 6Na^+ \\ &\qquad + NH_3 \end{aligned} \tag{2}$$

For the third reaction, the above process (reaction 1) is also repeated with minor changes; $SbCl_3$ is used in place of $Sb(CH_3COO)_3$; $KMnO_4$ is used together with hydrazine and NH_3 in place of NaOH. The pH of this mixture was around 10. The solids produced are a mixture of reddish brown and black in color:

$$\begin{aligned} &2SbCl_{3(aq)} + 3Na_2SeO_{3(aq)} \\ &\xrightarrow{N_2H_4+MnO_4{}^-{}_{(aq)}+NH_{3(aq)}} Sb_2Se_{3(s)}/Sb_{2-x}Mn_xSe_3 \\ &\qquad + MnO_{2(s)} + N_2 + 6Cl^- \\ &\qquad + 6Na^+ + NH_3 \end{aligned} \tag{3}$$

The pH of the permanganate solution was near neutral and unstable (reacts with water). The addition of NH_3 (weak base) made the solution basic and stable. At this pH, the permanganate solution is purple and stable and the manganese is mostly Mn(VII).

2.2. Characterization Techniques. The Sb_2Se_3 solids produced were characterized by X-ray powder diffraction (XRD) using a PANalytical X'Pert PRO X-ray diffractometer with a Cu-K_α radiation (40 KV, 30 mA), and a PIXcell solid state detector. The samples were prepared on glass sample holder. The patterns were recorded at room temperature with step sizes of 0.02°.

Surface structure and morphology of the sample were obtained with the aid of a Field Emission Scanning Electron Microscope (FESEM, Hitachi S-4200, Japan). The samples for FESEM analysis were prepared by suspending about 3 mg of the solid Sb_2Se_3 oxide in 1 mL of isopropanol. After the isopropanol was evaporated, the dry solid was placed on a double-sided black tape and then coated with sputtered platinum thin film prior to FESEM imaging.

Transmission electron microscopy (TEM) images were obtained with a Tecnai G^2 F20 S-Twin TEM instrument. The TEM operates at 200 KV using a field emission gun in Schottky mode as an electron source. The samples for TEM analysis were prepared by placing 3 mg of the air-dried solid Sb_2Se_3 in 10 mL of 2-propanol and sonication for 5 min for homogeneity. The holey carbon copper grid is dipped into the sonicated solution for a few seconds and then air-dried in the dark before analysis. UV-vis absorptions were carried out using a Shimadzu 160A (Japan) spectrophotometer. Photocatalytic performance of the Sb_2Se_3(s) rods and Sb_2Se_3(s) particles was evaluated by monitoring the decolorization of Rhodamine B in aqueous solution. The catalytic reaction is carried out in a 20 mL glass vial, which contained 10 mL of the Rh B (0.05 mM) dye solution and 15 mg of Sb_2Se_3 rods and/or $Sb_{2-x}Se_3$ particles. The mixture was allowed to react at 25°C under stirring. After reaction, the suspension was centrifuged and filtered and the supernatant analyzed using a UV-vis spectrometer (Shimadzu 160A UV, Japan). The efficiency of the catalysts is determined by difference in concentration of RhB between the initial and final readings at λmax = 501 nm.

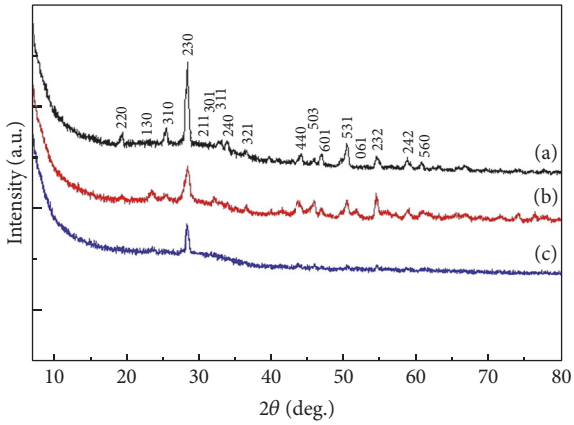

FIGURE 1: XRD patterns of ((a) and (b)) crystalline Sb_2Se_3 nanorods (reactions (1) and (2)) and (c) poorly crystalline Sb_2Se_3 nanoparticles (reaction (3)), prepared using hydrazine hydrate and MnO_4^- at 40°C with sonication for 40 min. For comparison, a theoretical XRD pattern for Sb_2Se_3 is shown.

3. Results and Discussion

3.1. Creation of Sb_2Se_3 Nanorods Using Hydrazine Hydrate ($N_2H_4{\cdot}H_2O$) and Morphological Changes Induced by Permanganate (MnO_4^-). The synthesis of Sb_2Se_3 nanorods consists of the reaction between $N_2H_4{\cdot}H_2O$ and SeO_3^{2-} in the presence of $Sb(CH_3COO)_3$ and/or $SbCl_3$ in near neutral and strongly basic media with incubation at 40°C and sonication for 30 min. In this complex reaction, $N_2H_4{\cdot}H_2O$ in basic aqueous solutions shows a strong reducing power according to the following redox reactions:

$$N_2H_4 + OH^- \longrightarrow N_2 + 4H_2O + 4e^- \quad E^o = 1.15\,V \tag{4}$$

$$Sb^{3+} + 3e^- \longrightarrow Sb \quad E^o = 0.20 \tag{5}$$

$$Se + 2e^- \longrightarrow Se^{2-} \quad E^o = -0.66 \tag{6}$$

In our experiments, $Sb(CH_3COO)_3$ and SeO_3^{2-} are used to react in molar ratios.

The temperature of 40°C was chosen because at this temperature a balance is maintained between minimum input of energy (more cost-effective) and a good product yield.

3.2. X-Ray Powder Diffraction, EDX, and XPS. The phases formed by the new method described above are characterized by XRD. Figure 1 shows the XRD patterns of ((a) and (b)) the crystalline nanorods of Sb_2Se_3 produced using $Sb(CH_3COO)_3$ and/or $SbCl_3$, Na_2SeO_3, and $N_2H_4{\cdot}H_2O$ with OH^- (reaction (1)) and without OH^- (reaction (2)) at 40°C and sonication for 40 min. These graphs indicate that the profile parameters of the diffraction peaks of the two types of Sb_2Se_3 produced by reactions (1) and (2) are very similar. The intensity of the peaks indicates that the samples are not highly crystalline. All peaks in Figures 1(a) and 1(b) can be indexed to an orthorhombic phase with lattice parameters: $a = 1.122$ nm, $b = 1.1128$ nm, and $c = 0.384$ nm with intensity and positions comparable with the values given in JCPDS (file card number: 15-861). The extra peak seen in Figure 1(b), at a 2θ value of 23.5°, is a result of a different orientation of the sample. It appears that no other phases are observed arising from impurities such as Sb_2O_3. Based on the standard redox potential shown in reactions (4), (5), and (6), the following possible redox half reactions (for reactions (1) and (2)) between N_2H_4 and SeO_3^{2-} are possible for the production of Sb_2Se_3 rods:

$$2Sb(CH_3COO)_3 + 3SeO_3^{2-} + N_2H_4 \cdot H_2O + OH^- \longrightarrow Sb_2Se_3 + N_2 + 4H_2O + NH_3 + 3CH_3COO^- \tag{7}$$

$$2SbCl_3 + 3SeO_3^{2-} + N_2H_4 \cdot H_2O \longrightarrow Sb_2Se_3 + N_2 + NH_3 + 4H_2O + 6Cl^- \tag{8}$$

The XRD pattern in Figure 1(c) reveals only the main peaks at around 25°–30°, suggesting the poorly crystalline nature of this sample obtained from reaction (3), where N_2H_4 and MnO_4^- are used together and $Sb(CH_3COO)_3$ is replaced with $SbCl_3$, respectively. Permanganate, which is an oxidizing agent, was used together with hydrazine firstly to slow down the reaction between hydrazine, $Sb(CH_3COO)_3$, and Na_2SeO_3, since this reaction is extremely fast at pH 10 and difficult to control, secondly to see the influence of permanganate in rod formation, and thirdly to see whether Mn^{2+} could be incorporated into the matrix of Sb_2Se_3 as an $Sb_{2-x}Mn_xSe_3$ doped material, since hydrazine is capable of reducing Mn^{7+} to Mn^{4+} and possibly even to Mn^{2+}. The XRD pattern for this reaction suggests that the choice of counter ions used for Sb when MnO_4^- is used is important to obtain a highly crystalline product. When this reaction was repeated using $SbCl_3$, the product was completely amorphous (not shown) with even more Mn content as impurity. It is clear from these results that Cl^- interferes with the redox process by channeling the reaction through a different pathway. It is also likely that Cl^- reacts with permanganate rather than with hydrazine to contribute to the observed effect. Thus, this reaction is very sensitive to experimental conditions used. Minor modification of the original procedure may result in the formation of mixed nanosized crystalline and poorly crystalline solids.

The element composition and purity of these nanomaterials were analyzed using EDXS. Figure 2(a) depicts typical EDX spectra recorded for the crystalline nanorods sample showing the presence of the elements Sb and Se. Interestingly, for the third reaction (not shown), the EDX pattern confirms the presence of Sb/Se and Mn as impurity for the Sb_2Se_3 particles, suggesting that MnO_4^- changed the crystallinity of the sample. Figure 2(b) shows a typical XPS survey spectrum of the as-prepared Sb_2Se_3 nanorods synthesized in the presence of hydrazine hydrate (reactions (1) and (2)) at 40°C and sonication for 40 min and suggests that the nanorods are composed of pure Sb and Se. The high resolution spectrum shown in Figures 2(b) and 2(c) indicates that the binding energies for Sb3d and Se3d in Sb_2Se_3 agree well with the published data [16].

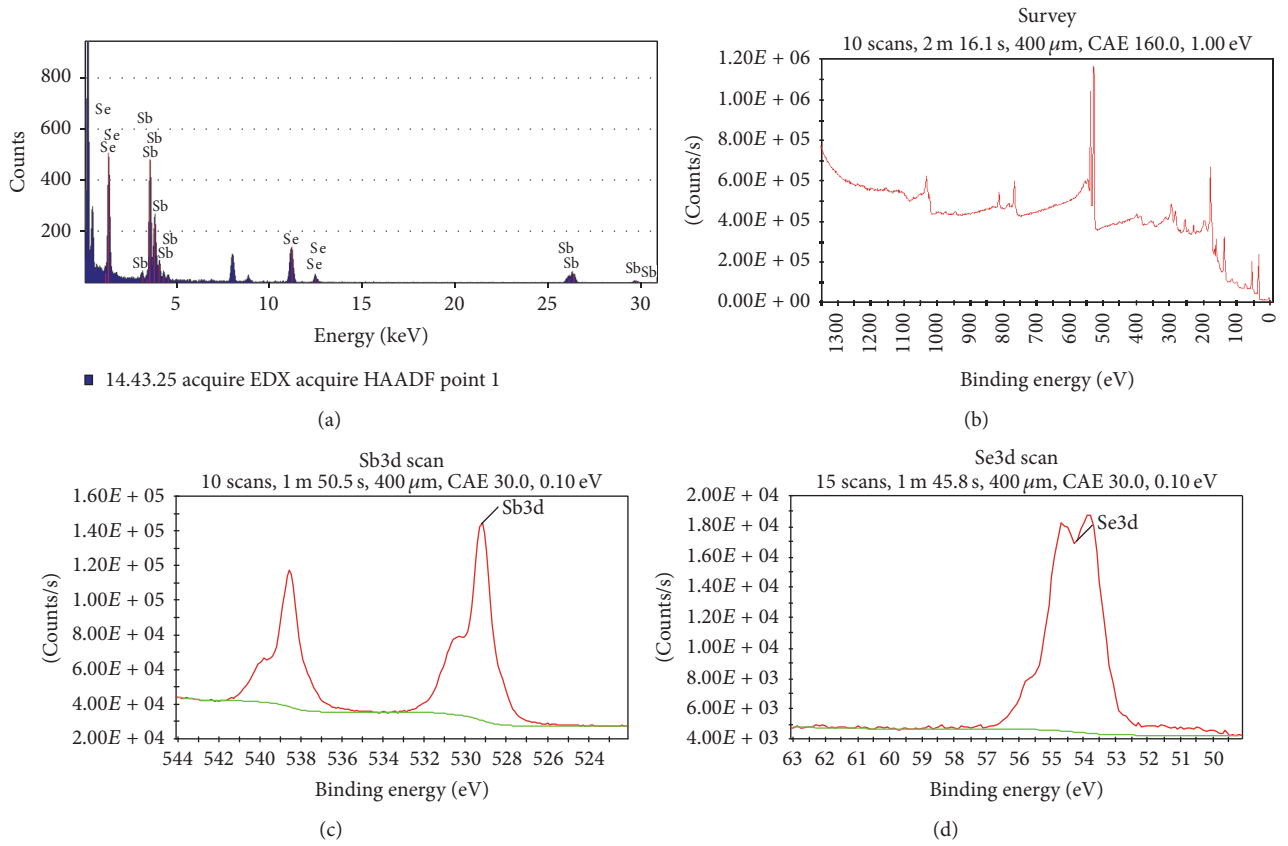

FIGURE 2: EDX and XPS spectra of the Sb_2Se_3 nanorods synthesized in the presence of hydrazine hydrate (reactions (1) and (2)) at 40°C and sonication for 40 min.: (a) typical EDX pattern, (b) typical XPS survey spectrum, and ((c) and (d)) close-up survey of the Sb3d core and Se3d core.

3.3. SEM, TEM, and HRTEM Studies. The nanostructures of both crystalline and poorly crystalline Sb_2Se_3 are studied using SEM, TEM, and HRTEM imaging. Figure 3 shows the SEM images of rods obtained for nanosized nanocrystalline and poorly crystalline Sb_2Se_3. For the crystalline samples (first and second reactions), (cf. Figures 3(a)–3(d)), the images show rods with orthorhombic shapes with lengths of about 100 nm to about 2 μm. Furthermore, the rods from the first reaction (cf. Figures 3(a) and 3(b)) appear thicker (0.1 μm) than the ones from the second reaction (0.05 μm) (cf. Figures 3(c) and 3(d)). We attribute this effect to the OH^- used in the first reaction (pH 10). At this solution pH, the production of solids is very fast, making the nanorods thicker. At near neutral pH, the production of solids is slower and this plus the salt type influences the size of the nanorods appearing thinner. The exact role of N_2H_4 in the formation of nanostructures is not known. We speculate that the role of N_2H_4 is both a reducing agent and a coordinator for the formation of the rod-like morphology. For the poorly crystalline sample (third reaction) (cf. Figures 3(e) and 3(f)), the images depict particles with bead-like shape with size of less than 20 nm that bundle together to form aggregates. In this reaction, it can be seen that the acetate and Cl^- (from $SbCl_3$) clearly affect the structure and morphology of the particles obtained, particularly when MnO_4^- is present. The effect of acetate is currently under investigation.

The TEM images shown in Figures 4(a)–4(f) display the crystal structure of the as-prepared Sb_2Se_3 nanorods (from the first and second reactions) and confirm the particle size of about 100 to 2 μm observed in the SEM images. The First Fourier Transform (FFT) patterns of the nanorods shown in the insets of Figures 4(c) and 4(f) suggest that Sb_2Se_3 obtained from the first and second reactions is indeed crystalline in nature with a growth direction. The SEM and TEM images also show that the products of the first and second reactions consist of mixtures of large (cf. Figure 4(a)) and small (cf. Figure 4(d)) nanorods, both of which appear faceted, with rectangular cross sections. Some of the rods in Figure 4(a) have stripes perpendicular to the nanorod axis. We speculate this to be a physical effect most likely due to local bending since the TEM images did not show any noticeable atomic disregistry across the glide plane.

The TEM and HRTEM images of the poorly crystalline Sb_2Se_3 are shown in Figures 4(g)–4(i). The TEM images display the bead-like distribution obtained for the light-colored Sb_2Se_3 particles with size of less than 20 nm. Some of these particles appear to bundle together to form nanoaggregates of about 100 nm. The SAED pattern (inset in Figure 4(i))

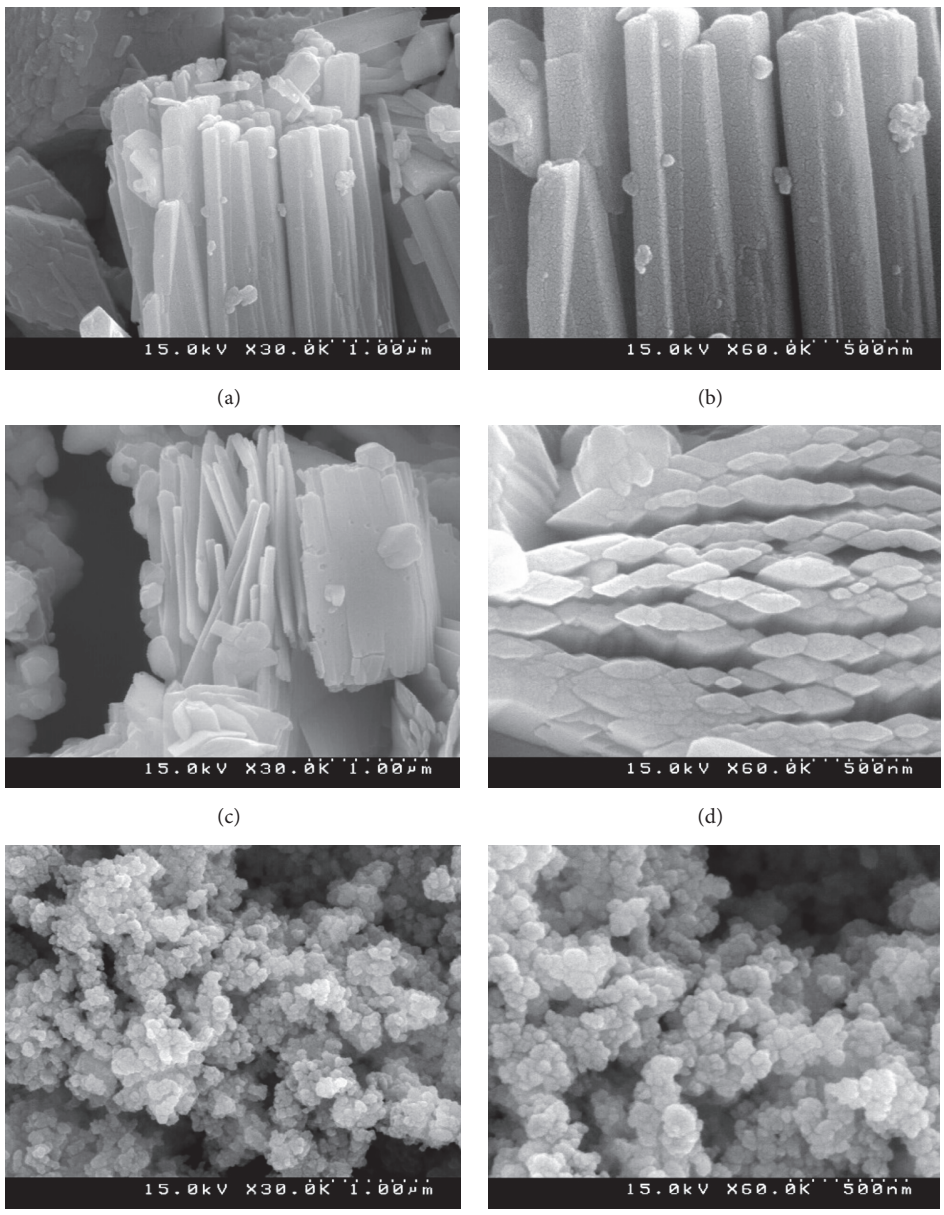

FIGURE 3: SEM images of ((a) and (b)) large crystalline Sb_2Se_3 nanorods (reaction (1)), ((c) and (d)) small crystalline Sb_2Se_3 nanorods (reaction (2)), and ((e) and (f)) poorly crystalline Sb_2Se_3 nanoparticles (at two different magnifications) prepared using hydrazine hydrate and MnO_4^- at 40°C and sonication for 40 min.

supports this observation as it indicates that there is no growth direction and suggests what appears as poorly crystalline to amorphous phase of Sb_2Se_3.

The XRD patterns and the TEM images confirm the structures of Sb_2Se_3 nanorods and suggest that the preferred ratio of Sb to Se is the one from the second reaction in which hydrazine hydrate was used in near neutral solution (cf. Figure 2(c)). We note that the redox-assisted formation of nanorods, in our system, is different from the chalcogenide nanoparticles formation by sheet rolling [23] and cation exchange reactions [24]. This "redox-assisted" synthesis of nanorods may permit the independent control of nanostructure composition and morphology by means of judiciously selecting counter ions for Sb(III) and hydrazine and MnO_4^- dose in the synthesis. The exact role of permanganate in reaction (3) is not known but we speculate that the acetate and Cl^- ions from Sb(III) play a more important role than was expected. It is clear that this may be the case in the third reaction where structural and morphological changes are induced by MnO_4^- by either incorporation of Mn into the lattice and/or coprecipitation of Mn during synthesis. Furthermore, the redox-stimulated shape evolution may

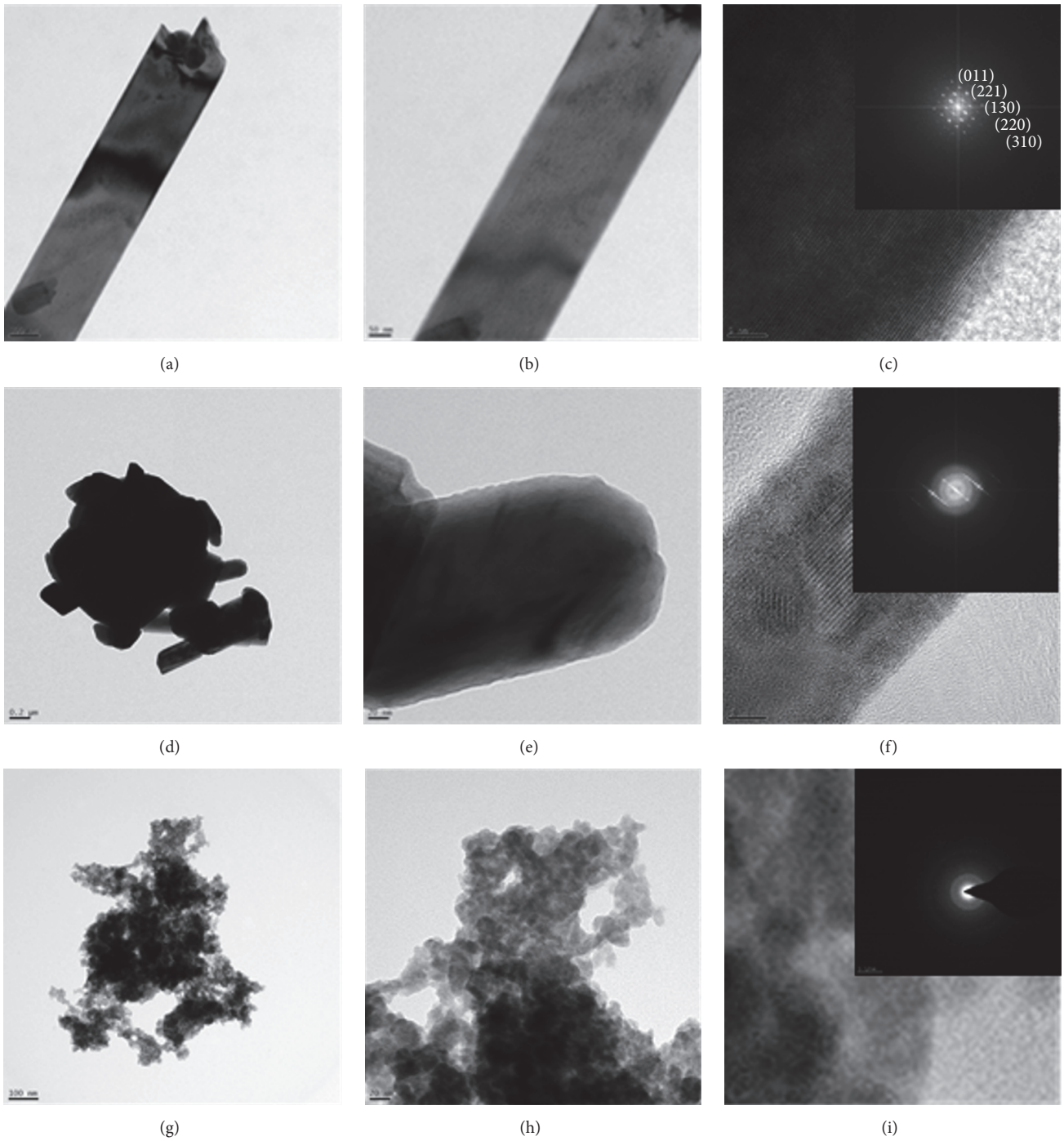

FIGURE 4: ((a), (b), and (c)) TEM and HRTEM images of the large crystalline Sb_2Se_3 nanorods (at three different magnifications); ((d), (e), and (f)) TEM and HRTEM images of the small crystalline Sb_2Se_3 nanorods; ((g), (h), and (i)) TEM and HRTEM image of the poorly crystalline Sb_2Se_3 nanoparticles. The insets in (c), (f), and (i) correspond to the FFT's and SAED patterns of a single Sb_2Se_3 nanorod and nanoparticle.

occur during nanostructure growth as a possible mechanism. The question as to why structural and morphological changes were induced by MnO_4^- is still under investigation. The best reproducible reaction condition for quantifying yield to produce in large scales depends on the size of the nanorods desired. For large nanorods, the first reaction is preferred, while for fine nanorods, the second reaction is recommended.

The UV-vis absorption spectrum of the crystalline and amorphous Sb_2Se_3 samples is shown in Figure 5. The spectrum of the crystalline samples shows an absorption maximum of 750 nm for reaction (1) and 760 nm for reaction (2), while the poorly crystalline samples show a maximum of 730 nm with corresponding band gaps of 1.65, 1.63, and 1.70 eV, respectively. This observation suggests a red shift

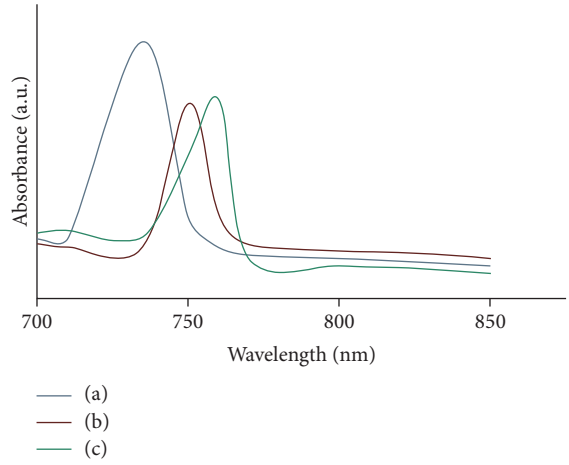

FIGURE 5: UV absorption patterns of the crystalline ((a) red and (b) green lines) Sb_2Se_3 nanorods and poorly crystalline ((c) blue line) Sb_2Se_3 nanoparticles.

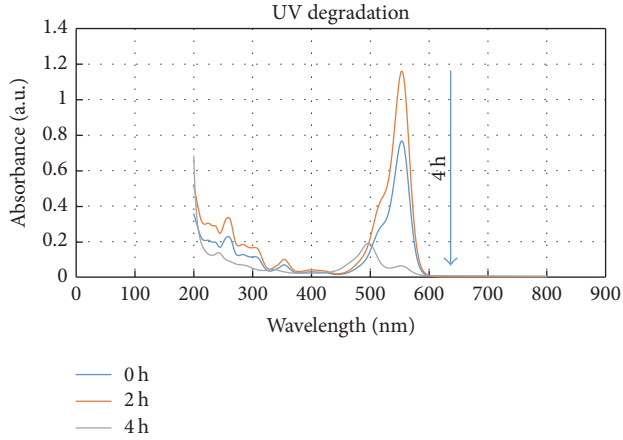

FIGURE 6: UV-vis absorbance spectra of RhB in solution after exposure to Sb_2Se_3 nanoparticles, in the presence of natural light, for 0, 2, and 4 h, respectively.

compared to the bulk sample consistent with common knowledge that the smaller the size of the particle, the higher the band gap. A solar cell under construction in our laboratory showed potential when Sb_2Se_3 was paired with CdS.

The efficiency of the semiconductor nanoparticles and nanorods with different band gap to function as photocatalyst was measured using RhB as a model organic pollutant in the presence of natural light. Figure 6 shows the UV absorption spectra of RhB in solution at different time intervals (0, 2, and 4 h) for nanoparticles (since decolorization of RhB by nanoparticles was slightly higher than nanorods; only results for nanoparticles are shown). In 2 h, about 50% of the RhB is decolorized followed by a 75% decolorization in 4 h. The photodecolorization of RhB by semiconductor nanoparticles may be explained by an adsorption-oxidation-desorption mechanism where oxygen accepts an electron forming a superoxide radical anion. These can react with water to form highly reactive hydroxyl radicals.

4. Conclusion

A new method using hydrazine hydrate and permanganate was developed to prepare Sb_2Se_3 nanorods and nanoparticles with uniform size and morphology. The use of hydrazine hydrate in basic solution (in the presence of selenite and antimony acetate) channels the reaction towards the production of large rod-like Sb_2Se_3 nanocrystals, while the use of hydrazine hydrate in near neutral solution (in the presence of selenite and antimony chloride) channels the reaction in the direction of producing small rod-like Sb_2Se_3 nanocrystals. The use of permanganate, hydrazine, $Sb(CH_3COO)_3$, and selenite produces Sb_2Se_3 nanocrystals with Mn as an impurity. One attractive feature for our system is that it is simple, cost-effective, and reproducible. Large scale production would depend on what is desired. For large nanorods, the first reaction is recommended, while for fine nanorods, the second reaction is best. The photocatalytic study demonstrated that semiconductor nanoparticles are more effective in the decolorization of RhB via possibly free radical formation. Antimony selenide nanoparticles may find potential application not only in thermoelectric, photovoltaic, and phase-change memory devices but also as catalyst for the transformation of organic pollutants.

Conflicts of Interest

The authors declare that they have no conflicts of interest.

Acknowledgments

This work was supported by the National Research Foundation of Korea (Grant NRF-2015-002423).

References

[1] X. W. Zheng, Y. Xie, L. Y. Zhu et al., "Growth of Sb_2E_3 (E = S, Se) polygonal tubular crystals via a novel solvent-relief-self-seeding process," *Inorganic Chememistry*, vol. 41, p. 455, 2002.

[2] N. S. Patil, A. M. Sargar, S. R. Mane, and P. N. Bhosale, "Growth mechanism and characterisation of chemically grown Sb doped Bi2Se3 thin films," *Applied Surface Science*, vol. 254, no. 16, pp. 5261–5265, 2008.

[3] S. Subramanian and D. P. Padiyan, "Effect of structural, electrical and optical properties of electrodeposited bismuth selenide thin films in polyaniline aqueous medium," *Materials Chemistry and Physics*, vol. 107, p. 392, 2008.

[4] C. Mastrovito, J. W. Lekse, and J. A. Aitken, "Rapid solid-state synthesis of binary group 15 chalcogenides using microwave irradiation," *Journal of Solid State Chemistry*, vol. 180, no. 11, pp. 3262–3270, 2007.

[5] S. K. Batabyal, C. Basu, A. R. Das, and G. S. Sanyal, "Solvothermal synthesis of bismuth selenide nanotubes," *Materials Letters*, vol. 60, no. 21-22, pp. 2582–2585, 2006.

[6] X. Qiu, C. Burda, R. Fu, L. Pu, H. Chen, and J. Zhu, "Heterostructured Bi2Se3 nanowires with periodic phase boundaries," *Journal of the American Chemical Society*, vol. 126, no. 50, pp. 16276-16277, 2004.

[7] Y. Jiang, Y. J. Zhu, and G. F. Cheng, "Synthesis of Bi_2Se_3 nanosheets by microwave heating using an ionic liquid," *Crystal Growth & Design*, vol. 6, p. 2174, 2006.

[8] S. Messina, M. T. S. Nair, and P. K. Nair, "Solar cells with Sb_2S_3 absorber films," *Thin Solid Films*, vol. 517, no. 7, pp. 2503–2507, 2009.

[9] Y. H. Kwon, M. Jeong, H. W. Do, J. Y. Lee, and H. K. Cho, "Liquid-solid spinodal decomposition mediated synthesis of Sb_2Se_3 nanowires and their photoelectric behavior," *Nanoscale*, vol. 7, no. 30, pp. 12913–12920, 2015.

[10] H. M. Yang, X. H. Su, and A. D. Tang, "Microwave synthesis of nanocrystalline Sb_2Se_3 and its electrochemical properties," *Materials Research Bulletin*, vol. 42, Article ID 421357, p. 1357, 2007.

[11] M. Lallakantouri, A. G. Marison, and G. E. Manoussakis, "Thermal decomposition of tris(*N*, N-disubstituted dithiocarbamate) complexes of As(III), Sb(III) and Bi(III)," *Journal of Thermal Analysis*, vol. 29, no. 5, pp. 1151–1169, 1984.

[12] Y. Yang, H. Zeng, S. H. Yu, L. Yang, and Y. H. Zhang, "Pressure-controlled fabrication of stibnite nanorods by the solvothermal decomposition of a simple single-source precursor," *Chemistry of Materials*, vol. 12, no. 10, pp. 2924–2929, 2000.

[13] W. J. Lou, M. Chen, X. B. Wang, and W. M. Liu, "Novel single-source precursors approach to prepare highly uniform Bi_2S_3 and Sb_2S_3 nanorods via a solvothermal treatment," *Chemistry of Materials*, vol. 19, no. 4, pp. 872–878, 2007.

[14] O. Savadogo and K. C. Mandal, "Studies on new chemically deposited photoconducting antimony trisulphide thin films," *Solar Energy Materials and Solar Cells*, vol. 26, no. 1-2, pp. 117–136, 1992.

[15] D. Choi, Y. Jang, J. Lee et al., "Diameter-controlled and surface-modified Sb2Se3 nanowires and their photodetector performance," *Scientific Reports*, vol. 4, article 6714, 2014.

[16] Y. Q. Liu, M. Zhang, F. X. Wang, and G. B. Pan, "Facile microwave-assisted synthesis of uniform Sb_2Se_3 nanowires for high performance photodetectors," *Journal of Materials Chemistry C*, vol. 2, no. 2, pp. 240–244, 2014.

[17] X. C. Ma, Z. D. Zhang, X. Wang, S. T. Wang, F. Xu, and Y. T. Qian, "Large-scale growth of wire-like Sb_2Se_3 microcrystallines via PEG-400 polymer chain-assisted route," *Journal of Crystal Growth*, vol. 263, p. 491, 2004.

[18] S. K. Batabyal, C. Basua, G. S. Sanyal, and A. R. Das, "Synthesis of Sb_2Se_3 nanorods using B-cyclodextrin," *Materials Letters*, vol. 58, pp. 169–171, 2003.

[19] D. B. Wang, C. X. Song, X. Fu, and X. Li, "Growth of one-dimentional Sb_2Se_3 and Sb_2Se_3 crystals with straw-tied like architectures," *Journal of Crystal Growth*, vol. 28, p. 611, 2005.

[20] Q. Xie, Z. P. Liu, M. W. Shao, L. F. Kong, W. C. Yu, and Y. T. Qian, "Polymer-controlled growth of Sb_2Se_3 nanoribons via a hydrothermal process," *Journal of Crystal Growth*, vol. 252, p. 570, 2003.

[21] J. W. Wang, Z. X. Deng, and Y. D. Li, "Synthesis and characterization of Sb_2Se_3 nanorods," *Materials Research Bulletin*, vol. 37, no. 3, pp. 495–502, 2002.

[22] D. B. Wang, D. B. Yu, M. S. Mo, X. M. Liu, and Y. T. Qian, "Preparation and characterization of wire-like Sb_2Se_3 and flake-like $B_{12}Se_3$ nanocrystals," *Journal of Crystal Growth*, vol. 253, p. 445, 2003.

[23] M. Bar-Sadan, I. Kaplan-Ashiri, and R. Tenne, "Inorganic fullerenes and nanotubes: wealth of materials and morphologies," *European Physical Journal: Special Topics*, vol. 149, no. 1, pp. 71–101, 2007.

[24] B. Zhang, Y. Jung, H.-S. Chung, L. Van Vugt, and R. Agarwar, "Nanowire transformation by size-dependent cation exchange reactions," *Nano Letters*, vol. 10, no. 1, pp. 149–155, 2010.